JOURNAL OF GEOPHYSICAL RESEARCH, VOL. 115, E05006, doi:10.1029/2009JE003396, 2010

Martian dust devil electron avalanche process and associated electrochemistry

Telana L. Jackson,[1] William M. Farrell,[1] Gregory T. Delory,[2] and Jeyasingh Nithianandam[3]

Received 3 April 2009; revised 8 December 2009; accepted 18 December 2009; published 22 May 2010.

[1] Mars' dynamic atmosphere displays localized dust devils and larger, global dust storms. Based on terrestrial analog studies, electrostatic modeling, and laboratory work, these features will contain large electrostatic fields formed via triboelectric processes. In the low-pressure Martian atmosphere, these fields may create an electron avalanche and collisional plasma due to an increase in electron density driven by the internal electrical forces. To test the hypothesis that an electron avalanche is sustained under these conditions, a self-consistent atmospheric process model is created including electron impact ionization sources and electron losses via dust absorption, electron dissociation attachment, and electron/ion recombination. This new model is called the Dust Devil Electron Avalanche Model (DDEAM). This model solves simultaneously nine continuity equations describing the evolution of the primary gaseous chemical species involved in the electrochemistry. DDEAM monitors the evolution of the electrons and primary gas constituents, including electron/water interactions. We especially focus on electron dynamics and follow the electrons as they evolve in the *E* field driven collisional gas. When sources and losses are self-consistently included in the electron continuity equation, the electron density grows exponentially with increasing electric field, reaching an equilibrium that forms a sustained time-stable collisional plasma. However, the character of this plasma differs depending upon the assumed growth rate saturation process (chemical saturation versus space charge). DDEAM also shows the possibility of the loss of atmospheric methane as a function of electric field due to electron dissociative attachment of the hydrocarbon. The methane destruction rates are presented and can be included in other larger atmospheric models.

Citation: Jackson, T. L., W. M. Farrell, G. T. Delory, and J. Nithianandam (2010), Martian dust devil electron avalanche process and associated electrochemistry, *J. Geophys. Res.*, *115*, E05006, doi:10.1029/2009JE003396.

1. Introduction

[2] Previous studies show that terrestrial dust devils can generate large coherent electrostatic fields through triboelectric interactions involving grains of dust and sand [*Freier*, 1960; *Crozier*, 1964]. It has been predicted through theoretical models that Martian dust devils may have large electrostatic fields, with their magnitudes approaching atmospheric breakdown levels of ~25 kV/m [*Melnik and Parrot*, 1998; *Farrell et al.*, 2003, 2006b; *Zhai et al.*, 2006]. These dust devil electric fields are formed through contact electrification, where larger sand and smaller dust grains collide with each other and the surface, generating and transferring electrical charge through friction [*Ette*, 1971; *Melnik and Parrot*, 1998; *Desch and Cuzzi*, 2000; *Farrell et al.*, 2003]. This process leaves smaller dust particles with a net negative charge and larger sandy grains and the surface with a net positive charge [*Ette*, 1971; *Jackson and Farrell*, 2006; *Kok and Renno*, 2008; *Forward et al.*, 2009].

[3] Vertical winds in the storm then mass stratify (and charge stratify) the grain distribution as a function of height, creating a downward directed electric dipole moment and a large-scale dipole electric field in the atmosphere [*Crozier*, 1964; *Farrell et al.*, 2004]. Under the influence of these large-scale driving electric fields, low-pressure Martian CO_2 gas can be a source of electrons through an impact ionization process which may become sufficient to create an electron avalanche and sustain a collisional plasma within the active dust column. Figure 1 is a composite image showing the electric field, positive and negative charge separation, and electrons interacting with the CO_2 gas. The prospect of such activity was originally described by *Mills* [1977] and expanded by *Delory et al.* [2006] and *Atreya et al.* [2006]. We now present a modeling advancement that couples

[1]Solar System Exploration Division, NASA Goddard Space Flight Center, Greenbelt, Maryland, USA.
[2]Space Sciences Laboratory, University of California, Berkeley, California, USA.
[3]Department of Electrical Engineering, Morgan State University, Baltimore, Maryland, USA.

0148-0227/10/2009JE003396

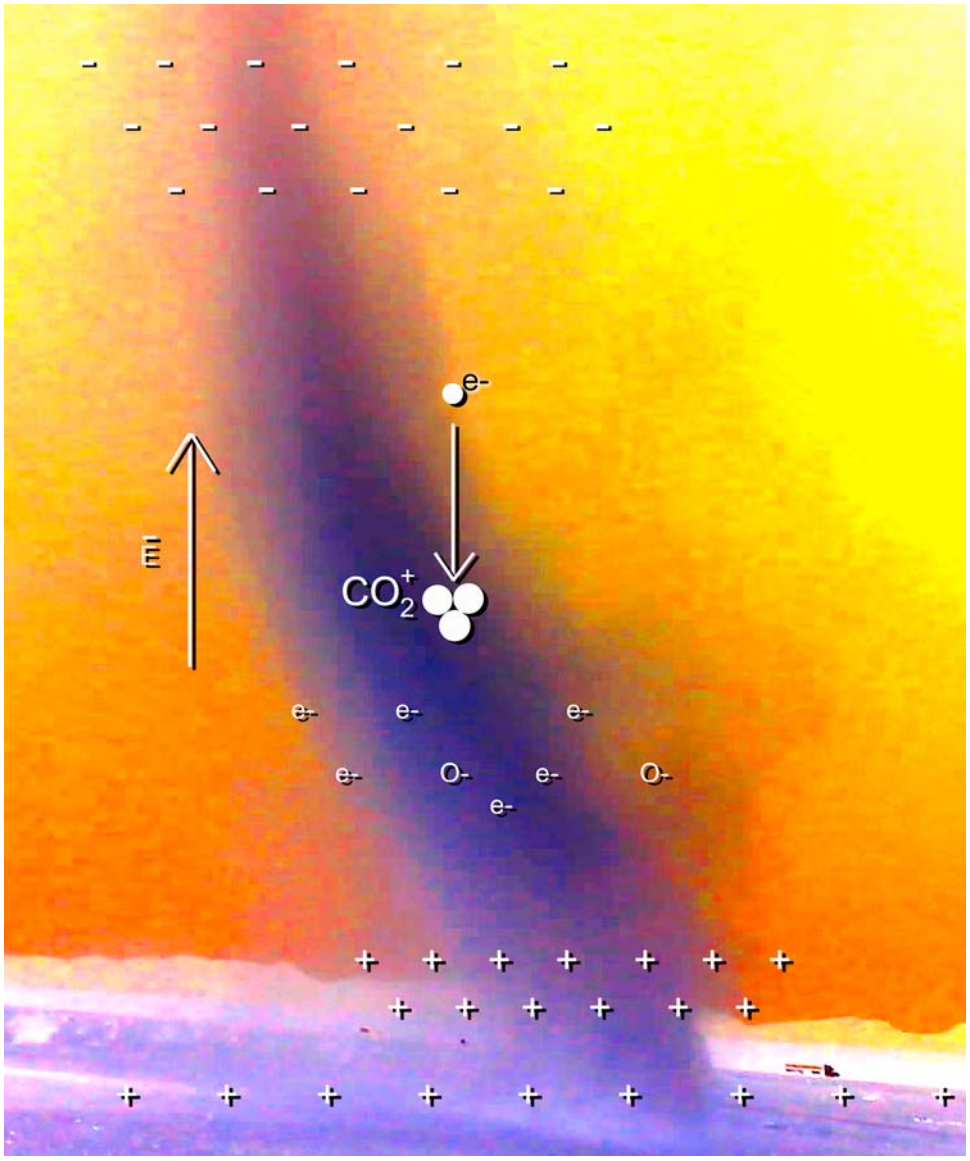

Figure 1. A dust devil with the downward facing electric field. Negative charge is at the top of the structure, and positive charge is on the bottom and at the surface. Electrons within the dust devil collide with ambient CO_2 and dissociate the molecules creating more electrons and O^-.

continuity equations for electrons and applicable chemical species and includes electron loss processes such as electron/ion recombination and electron/dust absorption.

[4] Models of Martian dust storms predict that they form well-defined charge centers: negative charge (−) at the top and positive charge (+) at the bottom. Electrostatic fields consistent with this picture have been measured in terrestrial dust devils [*Crozier*, 1964; *Farrell et al.*, 2003; *Jackson and Farrell*, 2006] and it is expected that Martian dust devils and convective storms will also develop large-scale E fields. In the low-pressure Martian atmosphere, these electric forces can then accelerate ambient electrons in the Martian atmosphere and these electrons will then collide with the atmospheric gas molecules to create new chemistry [*Delory et al.*, 2006]. An electron can collisionally ionize a CO_2 molecule if it has an energy exceeding 14 eV. This ionization process releases additional electrons that also get accelerated to thereafter ionize other molecules. In essence, the E field starts a chain reaction or an electron "avalanche" that creates a nonthermal electron population [*Delory et al.*, 2006].

[5] Examples based on laboratory results further confirm this picture of a dusty electrical Martian gas. *Eden and Vonnegut* [1973] stirred dust and sand in a CO_2 gas under Martian-like pressure and indeed found that the gas developed both a diffuse glow and created filamentary discharges to the wall of the container. The glow discharge suggests that an electron population is present with energies close to 10 eV, the excitation energy of CO_2. *Mills* [1977] performed a similar test and also detected a glow discharge in the dusty CO_2 low-pressure gas. The creation of a collisional plasma so impressed Mills that he suggested that the electron

chemistry associated with the process might "scavenge" the surface of organics. The *Delory et al.* [2006] and *Atreya et al.* [2006] papers further quantify this process.

[6] There are three primary reactions that affect the electron avalanche process in the Martian atmosphere. The first process is an electron source in the gas called electron impact ionization (EII): For every one electron with an energy u > 14 eV incident with a neutral CO_2, two electrons are produced with the ion ($e + CO_2 = 2e + CO_2^+$). These two new electric field driven electrons then collide with two other neutrals, resulting in four electrons, etc. In this way, an electron avalanche is created. The second process, creating a loss of electrons, is electron/CO_2 dissociative attachment (ED of CO_2), where the electron of specific energy interacts with the CO_2 molecule and divides the molecule, creating CO and O^-. The reaction ($e + CO_2 = CO + O^-$) occurs in a relatively narrow energy band near 4.4 eV. The third process, also an electron loss process, is called electron/CO_2^+ recombination (ER). The electron incident with the CO_2^+ ion recombines to create a neutral CO_2 molecule ($e + CO_2^+ = CO_2$). If the electron avalanche process becomes large, it can offset the losses and create a large electron concentration. We demonstrate that in fact the avalanche process can stabilize into a sustained collisional plasma within the dust devil.

[7] A complementary set of papers by *Delory et al.* [2006] and *Atreya et al.* [2006] examined the behavior of ambient electrons in the Martian atmosphere under the influence of large *E* fields (like that in dust devils/storms/fronts). It was found that the electrons evolve in three ways: First, a distinct high-energy electron tail develops in the electron energy distribution, with its power law roll-off in the tens of eVs decreasing directly with increasing E [*Nighan*, 1970; *Delory et al.*, 2006]. Second, due to this energetic electron tail, the electron density increases geometrically with increasing driving *E* field, due to the increasing number of CO_2 impact ionizations from the presence of the greater number of electrons with u > 14 eV. Finally, the electron drift velocity steadily increases with E reaching ~2×10^5 m/s above 10 kV/m.

[8] *Delory et al.* [2006] solved the Boltzmann equation using the *Pitchford et al.* [1981] solution for the electron energy distribution functions as a function of E in the CO_2 gas. Using these distributions, Townsend's first coefficient was derived. Townsend's first coefficient defines the electron growth through impact ionization as a function of driving *E* field in the CO_2 gas. The electron density in a lossless medium varies as $e^{\alpha z}$ where α is Townsend's first coefficient. The inverse of α describes the mean free path length between electron impact ionizations. If the length of the coherent *E* field stressing the gas is L, then a geometric increase in electron density can occur for $\alpha \gg 1/L$. For low *E* field values below 10 kV/m, the electron growth length ($1/\alpha$) is very large and exceeds the size of a typical dust devil. However, for large *E* field values above 15 kV/m, electron impact ionization can create a second ionized electron in a spatial scale of less than a meter creating substantial growth. *Delory et al.* [2006] also found that this energetic electron population (possessing a discernable tail in its energy distribution) could easily modify CO_2 into CO and O^- through electron dissociation attachment near 4.4 eV [*Itikawa*, 2002] and could also divide water into OH and H^- also via electron dissociative attachment near 6.5 eV. In essence, Delory et al. created an analytical model of the "scavenging electron gas" (envisioned by *Mills* [1977]) that could put quantifiable values on the electron density, electron velocity, and subsequent new chemical products CO, OH, O^- and H^-. These *E* field enhanced species then were used as inputs into a larger atmospheric chemistry model [*Atreya et al.*, 2006] which found that the mixing Os and Hs create HO_2 and thus enhanced concentration of H_2O_2 at levels 20–200 times greater than that of simple photochemistry processes alone.

[9] The Delory/Atreya pathfinding model suggested that there are new active electrochemical pathways on Mars, especially during extreme storm conditions, that were not been previously appreciated. *Farrell et al.* [2006b] demonstrated that the dust storm energetic electron population >10 eV can in fact destroy methane through electron dissociative attachment processes. These findings suggest that dust electrochemistry is a sink of this important molecular biosignature.

[10] In the study herein, the primary objective is to expand the original model created by *Delory et al.* [2006] by including not only electron impact ionization sources but also a set of electron loss processes such as dust absorption, electron recombination and electron dissociative attachment. These dust storm electron losses have not been included in previous models and should greatly enhance the findings of *Delory et al.* [2006] in describing the electron avalanche process. The only other work that has included loss processes is that of *Kok and Renno* [2009] which compliments this work. In their case, they considered tribocharging and associated plasma chemistry of large grains (~100 microns) in the spatially limited saltation region. The study presented here considers the spatially larger region where dust devil electric fields exist. Included herein is also the consideration of saturation mechanisms that ultimately limit the electron avalanche.

2. Approach

[11] The first step defining the electron avalanche process is to obtain the electron energy distribution in the CO_2 gas under the influence of the driving electrostatic field. This can be modeled with the Boltzmann equation $\frac{\partial f}{\partial t} + \overline{v} \cdot \overline{\nabla} f + \frac{\overline{F}}{m} \frac{\partial f}{\partial \overline{v}} = \left(\frac{\partial f}{\partial t}\right)_c$ [*Chen*, 1984], where f is the velocity distribution, $\overline{v}$ is the velocity vector, $\overline{F} = q\overline{E}$ is the force acting on the particles, m is particle mass and $\left(\frac{\partial f}{\partial t}\right)_c$ represents effects due to electron/molecule collisions. The collision term on the right-hand side of the equation is unique to each gas species, and for CO_2 is illustrated by *Itikawa* [2002, Figure 20]. At low energies below ~1 eV, elastic collisions (momentum transfer) between the electron and individual C and O nuclei define the cross section. At higher energies above 14 eV, inelastic collisions created by (e, CO_2) ionizations define the electron/molecule interactions and hence define the cross section values. Near 4 eV, the cross section is dominated by a set of CO_2 vibration modes that can be excited via inelastic electron collisions.

In general inelastic collisions have a noticeable effect on any electron energy distribution, tending to reinject an originally high-energy electron (located in the tail of the distribution) back into the low-energy core or "swarm." As such, inelastic collisions tend to make the electron distribution deviate from a simple Maxwellian distribution.

[12] The electron energy distribution, $f(u, E)$ was calculated previously using numerical methods by *Nighan* [1970] and *Delory et al.* [2006] for a low-pressure CO_2 atmosphere (the variable u is energy in eVs). Because the inelastic collision occurs at energies that are distributed between 1 and 14 eV, the electron energy distribution does approximately fit a straight line on a ln(f) versus u plot (i.e., appears similar to a Maxwellian distribution), with some relatively minor deviations near 3–4 eV where inelastic collisions excite vibration modes. Consequently, most of the distribution can be fit with the following simple expression $f(u, E) = f_o(u_o)e^{-2.3B(u-u_o)_E}$ where $f_o = 0.1$ eV$^{-3/2}$, B = 3880 V/meV, and u_o is 3 eV, an expression that holds for electron energies >0.2 eV and for E field values >5 kV/m [*Jackson*, 2008; *Jackson et al.*, 2008].

[13] Using the analytical $f(u, E)$, the objective is to derive an analytical expression for Townsend's first coefficient for ionization ($\alpha = \frac{n_{CO_2} k_i}{v_D}$) which is a function of the chemical rate of impact ionization k_i, and drift velocity v_D. The electron drift velocity (v_D) and the chemical rate of impact ionization (k_i) are themselves a function of the electron energy distribution, $f(u, E)$, and hence using the simplified form of the distribution it is easy to derive an analytical form. This derivation was presented previously by *Jackson et al.* [2008] and outlined in Appendix A. Using k_i and v_D, Townsend's first coefficient is found to be [*Jackson*, 2008; *Jackson et al.*, 2008] $\alpha(E) = -{n_{CO_2}}^2 \sigma_{el} \frac{C}{B} e^{-2.3\frac{B}{E}u_i}$ where the ionization energy $u_i = 14.5$ eV, $C = -1.3 \times 10^{-20}$ m^2, $\sigma_{el} = 0.84 \times 10^{-19}$ m^2 and $n_{CO_2} \cong 2 \times 10^{23}$ m^{-3} (see Appendix A). This analytical version scales with that of *Delory et al.* [2006].

[14] Previously, *Jackson* [2008] and *Jackson et al.* [2008] found a critical E field for the triggering of the electron avalanche by setting the electron source term (α) equal to a dust loss term η formulated therein (and described further below). In order to create the electron avalanche, a critical electric field has to be exceeded, thereby making the electron sources greater than the electron losses. If dust storm charge centers create an electric field below the $E_{critical}$ value ($\frac{dn_e}{dt} < 0$), the rate at which the electron density changes with respect to time is less than or equal to zero, and the dust in the devil/storm is absorbing the electrons faster than impact ionization creation. However, if the critical electric field is exceeded, then the electron density growth rate is greater than zero ($\frac{dn_e}{dt} > 0$) and the electron avalanche commences.

[15] In this work, we continue to expand our understanding of the processes that control the electron avalanche process in a dusty low-pressure CO_2 gas. We now analyze the electron continuity equation applying an impact ionization source term (i.e., applying the new simplified from of Townsend's first coefficient) but also including a number of loss terms, including dust absorption of electrons, electron recombination with resident CO_2 ions, and electron dissociative attachment with neutral CO_2. We find that the determination of evolution of electron density with time is highly dependent upon the concentration of carbon dioxide molecules and ions present at any given time, requiring a set of coupled equations that are solved simultaneously. This approach to derive the electron evolution is the essence of the present work.

3. Dust Devil Electron Avalanche Model

[16] A few assumptions were made in developing the DDEAM model. This zero-dimensional model of the temporal evolution of a fluid element in a dust devil/storm solves for the concentration of electrons as well as other relevant chemical species and products for two separate cases: the first case limiting concentrations via intrinsic chemistry, and the second via polarization currents in the plasma. The evolution of these concentrations is followed under a driving E field assumed to form independently via dust storm charge centers.

[17] In its simplest form, electrons and CO_2 interact through impact ionization, electron recombination, and electron dissociative attachment, described by reactions (1), (2), and (3) below. In this work we also consider the dissociative attachment of water (e, H_2O) that makes new species OH, and H^-, described by chemical equation (4).

$$e + CO_2 \rightarrow 2e + CO_2^+ \text{ u} \sim 14.5 \text{ eV (EII)} \quad (1)$$

$$e + CO_2^+ \rightarrow CO_2 \text{ u} \sim \text{thermal energy (ER)} \quad (2)$$

$$e + CO_2 \rightarrow CO + O^- \text{ u} \sim 4.4 \text{ eV (ED of } CO_2\text{)} \quad (3)$$

$$e + H_2O \rightarrow OH + H^- \text{ u} \sim 6.6 \text{ eV (ED of } H_2O\text{)} \quad (4)$$

[18] These chemical equations can be translated into coupled differential equations, thereby allowing a self-consistent solution of the electron continuity equation. We follow the evolution of electrons under a driving E field assumed to form via dust storm charge centers. These equations are the basis for the Dust Devil Electron Avalanche Model (DDEAM) developed in this work. The system of coupled equations that describe the electron evolution in a low-pressure CO_2 gas is [*Jackson*, 2008]

$$\frac{\partial n_e}{\partial t} = (\alpha(E) - \eta) n_e v_D - k_{CO_2^+/e} n_{CO_2^+} n_e - k_{CO_2/e} n_{CO_2} n_e - k_{H_2O/e} n_{H_2O} n_e - \frac{v_D n_e}{d} \quad (5)$$

$$\frac{\partial n_{CO_2^+}}{\partial t} = \alpha(E) n_e v_D - k_{CO_2^+/e} n_{CO_2^+} n_e \quad (6)$$

$$\frac{\partial n_{CO_2}}{\partial t} = -k_{CO_2/e} n_{CO_2} n_e - \alpha(E) v_D n_e + k_{CO_2^+} n_{CO_2^+} n_e \quad (7)$$

$$\frac{\partial n_{CO}}{\partial t} = k_{CO_2/e} n_{CO_2} n_e \quad (8)$$

$$\frac{\partial n_{O^-}}{\partial t} = k_{CO_2/e} n_{CO_2} n_e \quad (9)$$

$$\frac{\partial n_{H_2O}}{\partial t} = -k_{H_2O/e} n_{H_2O} n_e \quad (10)$$

$$\frac{\partial n_{OH}}{\partial t} = k_{H_2O/e} n_{H_2O} n_e \quad (11)$$

$$\frac{\partial n_{H^-}}{\partial t} = k_{H_2O/e} n_{H_2O} n_e \quad (12)$$

[19] The values $n_{CO_2^+}$, n_{CO_2} and n_{H_2O} correspond to the densities (in units of m^{-3}) of CO_2^+, CO_2 and H_2O. The chemical rates $k_{CO_2^+/e}$, $k_{CO_2/e}$ and $k_{H_2O/e}$ correspond to the electron/CO_2^+ recombination, electron/CO_2 dissociative attachment and electron/H_2O dissociative attachment processes, respectively, and are calculated to be $k_{CO_2^+/e} = \sim 2 \times 10^{-13}$ m^3/s, $k_{CO_2/e} = 0.39 \times 10^{-16} e^{-12493/E}$ m^3/s, and $k_{H_2O/e} = 0.25 \times 10^{-14} e^{-321264/E}$ m^3/s (see Appendix A for chemical rate calculations). The key equation is the electron continuity equation, equation (5) which contains the electron impact ionization source term ($\alpha n_e v_d$), a dust absorption loss term $\eta = n_D \sigma_D$ (a function of dust grain density and cross section that was analyzed recently by *Jackson et al.* [2008]), electron/CO_2^+ recombination loss term ($k_{CO_2^+/e} n_{CO_2^+} n_e$), electron/$CO_2$ dissociative attachment term ($k_{CO_2/e} n_{CO_2} n_e$), electron/H_2O dissociative attachment loss term ($k_{H_2O/e} n_{H_2O} n_e$), and a scale size term ($\frac{v_D n_e}{d}$) where d is the system length. However, a unique solution of equation (5) clearly requires the simultaneous solutions to equations (6)–(10) describing the temporal evolution of CO_2, CO_2^+, and H_2O. Equation (6) is associated with the first and second chemical equations (equations (1) and (2)) and defines the growth of CO_2^+ through both impact ionizations and subsequent recombination. Equations (7)–(9) are the continuity equations defining the dissociative attachment of CO_2, via the third chemical equation (equation (3)). Equation (7) describes the temporal evolution of CO_2 in the presence of recombination sources, electron dissociative attachment, and impact ionization losses. Equation (8) describes the production of CO from (electron/CO_2) dissociative attachment processes, while equation (9) describes the production of O^- from this same process. Equations (10)–(12) are associated with the fourth chemical equation describing the electron dissociative attachment of ($e + H_2O \rightarrow OH + H^-$). Equation (10) describes the evolution of H_2O, while equations (11) and (12) describe the production of dissociated products OH and H^-.

[20] The driving electric field is assumed to be created independently through the formation of charge centers at the top and bottom of the dust devil. Models by *Melnik and Parrot* [1998] and *Farrell et al.* [2003, 2006b] indicate that the light, negatively charged grains are lifted by vertical winds to the upper portions of the dust devil while positively charged heavy grains and the positively charged surface create another charging center at the lower portion of the dust devil/storm. A dipolar E field then forms in the storm. Thus, a large-scale E field is initially defined to be a linearly varying function from E min at $t = 0$ and ending at E max at $t = t$ max. For the runs presented here, $\Delta E = E_{max} - E_{min}$ was 5 kV/m and t_{max} was 300 μs, with a time step of 50 ns. As our intent was to consider the loss of electrons in a situation where the E field is geometrically rising, this particular E field setup was chosen in order to replicate the E field associated with a tribocharging source like that modeled by *Farrell et al.* [2003, 2006a]. Note that this change in electric field over 300 μs is consistent with a tribocharging current source of 10–100 $\mu m/m^2$ in the lifting dust. Simulations were performed with E_{max} = 10, 15, 17.5, 20, 25, and 30 kV/m. For the full DDEAM equation set, equations (5)–(12) were then solved self-consistently, including the electron/H_2O dissociative attachment, electron/CO_2 dissociative attachment, electron/CO_2^+ recombination, dust losses and system size losses. The initial values for the densities are $n_e = 5 \times 10^6$ m^{-3}, $n_{CO_2} = 2 \times 10^{23}$ m^{-3}, $n_{H_2O} = 6 \times 10^{19}$ m^{-3}, and 0 m^{-3} for n_{CO}, $n_{CO_2^+}$, n_{O^-}, n_{OH} and n_{H^-}.

[21] We recognize that we are modeling a large system with a path length for electron growth of about 60 m ($L \sim v_D t_{max}$). Electron growth will not continue infinitely, and there are in fact a number of limiting processes to quench or saturate electron growth. First, the path length can be limited which will inherently limit the electron growth. This possibility was modeled by *Delory et al.* [2006] and *Kok and Renno* [2009], who considered limited system path lengths of tens of centimeters. Second, the intrinsic chemistry may in some way limit the electron growth through the recombination of CO_2 ions. Given the obvious analogy to predator-prey models, this would be similar to limiting the growth of predators via the loss of prey. To consider this possibility, we leave all environmental drivers constant and allow the chemistry to evolve to a natural chemically defined saturation point. Finally, given that energetic electrons are created, there should be the development of a polarization electric field from space charge that offsets the original driving (environmental) electric field. This third possibility of a current-defined saturation point is also considered herein, with electron currents being allowed to feedback into the driving electric field. We then compare the growth, quenching, and final equilibrium states for these saturation, growth-limiting processes.

4. Saturation via Intrinsic Chemistry

[22] Figure 2 shows the electron density resulting from the DDEAM model (equations (5)–(12)) including a dust loss term of $\eta = 0.031$ m^{-1}. The variable η represents the mean free path between electron/dust collisions and is thus equal to the dust density times dust geometric cross section [*Jackson et al.*, 2008]. The effective cross section may be smaller due to negative charging of the dust grains, therefore the geometric cross section used here for electron-dust interactions can be considered an "upper bound." The η value of 0.031 m^{-1} is applied since it corresponds to having 10 micron grains suspended in the dust cloud at concentrations of 100 grains/cm^3 or 10^8 grains/m^3 which is representative of Martian dust storms [*Melnik and Parrot*, 1998; *Farrell et al.*, 1999]. We neglect losses with respect to ion/dust interactions since the ion drift velocity is very

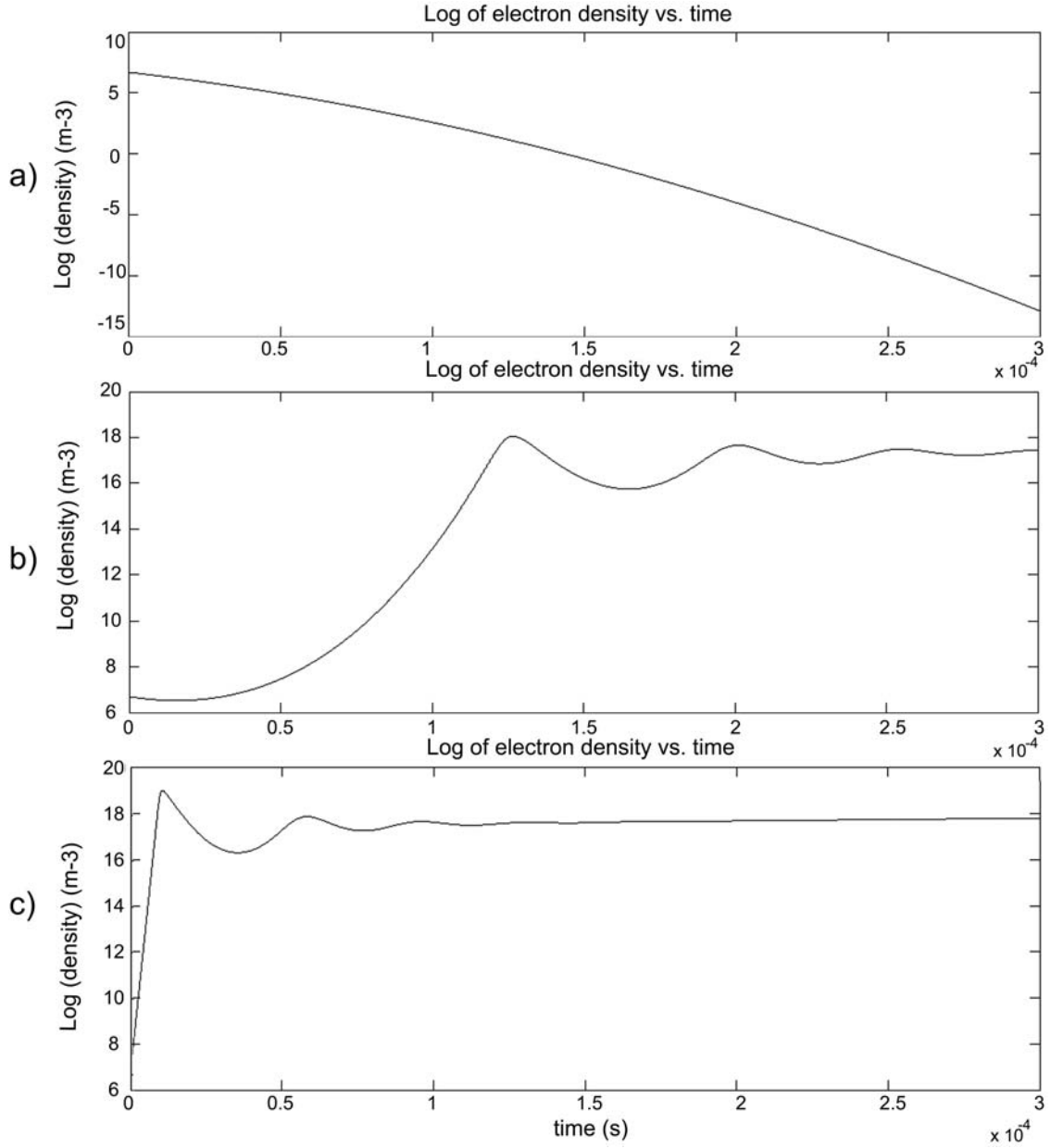

Figure 2. Electron density versus time for an E field (a) between 5 and 10 kV/m, (b) from 15 to 20 kV/m, and (c) from 20 to 25 kV/m, including a dust loss term with $\eta = 0.031$ m^{-1}.

slow in comparison to electrons. The model has the ability to consider various dust column sizes, d. The system scale size d was purposely set to a very large value for the cases presented herein. This choice was made so that the plasma chemistry could fully evolve in the simulation. Future work will be performed with new chemistry for various scale sizes (d from ~0.1–10 km), but is beyond the current scope of this work. However, for now we are more interested in the plasma chemistry effects rather than geometric effects. Cases for a low E field (5–10 kV/m), intermediate E field (15–20 kV/m) and high E field (20–25 kV/m) are presented in Figure 2.

[23] In Figure 2a, it is clear that there is no electron growth in the low E field, only electron loss through electron dissociative attachment. In these fields, an electron is created at a rate of $\alpha v_d \sim 10^3$/s while the attachment loss rate is $k_{CO_2/e} n_{CO_2} \sim 10^5$/s. Dust loss rates ηv_d are at 3100/s and play a secondary role. Recombination and system losses are not significant (system size is set to large values, purposely keeping that term small for this electrochemical comparison). However, in intermediate (Figure 2b) and large fields (Figure 2c), impact ionization sources initially exceed the losses, creating a situation where electron concentrations increase exponentially in time (called the growth or avalanche phase). The growth rates are steeper in larger fields, since $\alpha = \alpha(E)$ is also geometrically larger. As such, in intermediate fields, the electron avalanche process is slower, while in large fields the growth of electrons is

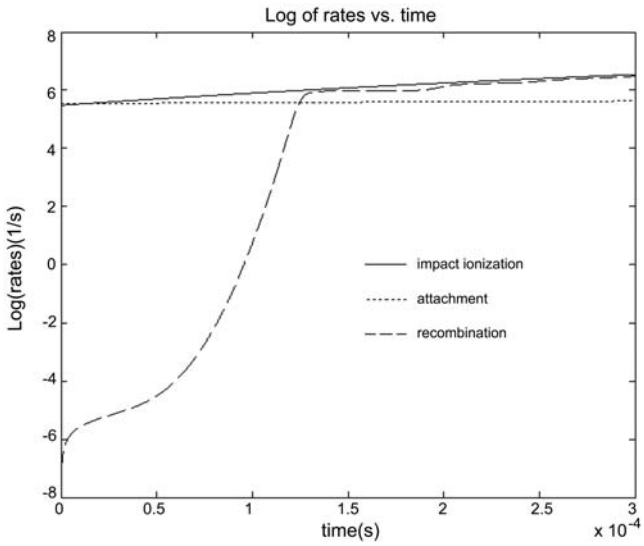

Figure 3. The rates of impact ionization (αv_d) (solid), attachment loss ($k_{CO_2/e} n_{CO_2}$) (dotted), and recombination ($k_{CO_2^+/e} n_{CO_2^+}$) (dashed) versus time for the intermediate field case E = 15–20 kV/m.

relatively fast. The growth of electrons in both cases proceeds at different rates to values near $10^{17}/m^3$, where the growth process saturates and the electrochemical system reaches a quasi-stable equilibrium. This period is called the saturation phase. The equilibrium point is nearly the same in each case that displays growth, only the rate to achieve this equilibrium differs under varying E (i.e., the slope of $\frac{dn_e}{dt}$ in the growth phase differs since it is a function of α(E)). The reason for the quenching of the avalanche process (or saturation) is due to the presence of copious amounts of CO_2^+ ions that recombine with the electrons.

[24] Figure 3 shows the rates of impact ionization (αv_d), attachment loss ($k_{CO_2/e} n_{CO_2}$) and recombination ($k_{CO_2^+/e} n_{CO_2^+}$) for the intermediate field case (15–20 kV/m). Initially, impact ionization rates exceed all losses, creating a period of steady growth. However, near 125 μs into the run, enough CO_2^+ is generated to limit electron growth through recombination. After this time, the impact ionization and recombination rates approximately track each other. As such, once in equilibrium, we can estimate the density of CO_2^+ ions as $n_{CO_2^+} \sim \alpha v_d / k_{CO_2^+/e} \sim 10^{19}/m^3$.

[25] One unanticipated result is evident for the intermediate and large field cases: A natural electron concentration oscillation develops as the system moves from an early growth/avalanche phase to a saturated state. Relative maxima can be seen in the intermediate case (Figure 2b) at 125 μs, 200 μs and 255 μs, with each maximum progressively reduced in amplitude. Similar relative maxima are observed in the large field case as well. Such oscillations represent a marginally stable situation where growth through electron impact ionization competes with the primary loss process of electron recombination that creates saturation (see also Figure 3). The DDEAM code was ran at various time steps with no evident change, suggesting that the time step does not affect the observed oscillations. Early in the saturation phase, these two effects do not exactly balance, but overcompensate and undercompensate giving rise to the relative maxima and minima in electron concentration. At later times they achieve an exact balance creating a $\frac{dn_e}{dt} = 0$ and hence a sustained collisional plasma.

[26] This marginal stability is not unprecedented: The character of the electron growth phase, saturation phase, and associated postgrowth oscillations are very reminiscent of plasma wave instabilities that form in homogenous collisionless plasmas. Simulations of plasma wave growth (that include the nonlinear coupling between waves and plasma particles) display a distinct growth phase where an energetically inverted population of particles drives the wave, a saturation point where the particle population feeding the waves is depleted, and oscillations in the early saturation phase where wave and particles interchange energy to achieve an equilibrium point [*Klimas and Farrell*, 1994]. As such, the oscillations in electron concentration (or current impulses) created by the DDEAM model of electron growth and saturation are believed to be a natural effect resulting from the nonlinearly coupled dynamic system of differential equations.

[27] Figure 4 shows the evolution of new species from the electron avalanche process for the case of a driving field between 15 and 20 kV/m and dust loss function η = 0.031 m^{-1}. Figure 4a shows the log of the electron density, CO_2 density and CO_2^+ density over time. The electron density grows for the first 125 μs and then stabilizes thereafter. The CO_2^+ density shows a similar trend as the CO_2 density decreases in cadence due to impact ionization. Figure 4b shows the log of the CO and O^- densities over time. The density of CO and O^- are the same and these products grow and reach a value of ~10^{19} m^{-3}. Figure 4c shows the log of the H_2O density over time and Figure 4d shows the log of the OH and H^- densities over time. The H_2O density decreases since it is being dissociated by the energetic electrons and the products of this dissociation, OH and H^-, have the same density, growing to a value of ~10^{16} m^{-3}.

[28] Table 1 shows the final density values for electrons, CO_2, and dissociative attachment products CO and O^-, water, and dissociative attachment products OH and H^-, CO_2^+ and change in CO_2 density over time as a function of the driving electric field for given runs. For *E* fields less than ~15 kV/m, the dissociative attachment process effectively absorbs the energetic electrons, creating an overall electron loss in the system (see Figure 2a). However, above ~15 kV/m, the creation of electrons through impact ionization offsets the attachment losses and the electron concentrations are found to grow, stabilizing at equilibrium values at about 3 ppm.

[29] We note that in larger fields, the energetic electrons have an affinity for dissociative attachment to CO_2, with the electrons becoming attached to the dissociated oxygen, creating copious amounts of O^- ions. In equilibrium, the O^- ions are nearly at 0.1% of the atmospheric content and are the primary "keeper" of the system's negative charge. As described by *Atreya et al.* [2006], we fully anticipate that the O^- and H^- ions further react to create other species, including peroxides.

[30] Like CO_2 and H_2O, methane is also a molecule that undergoes dissociative attachment through the energetic electron avalanche process in a dust storm [*Farrell et al.*, 2006b]. The methane loss rate, which was added

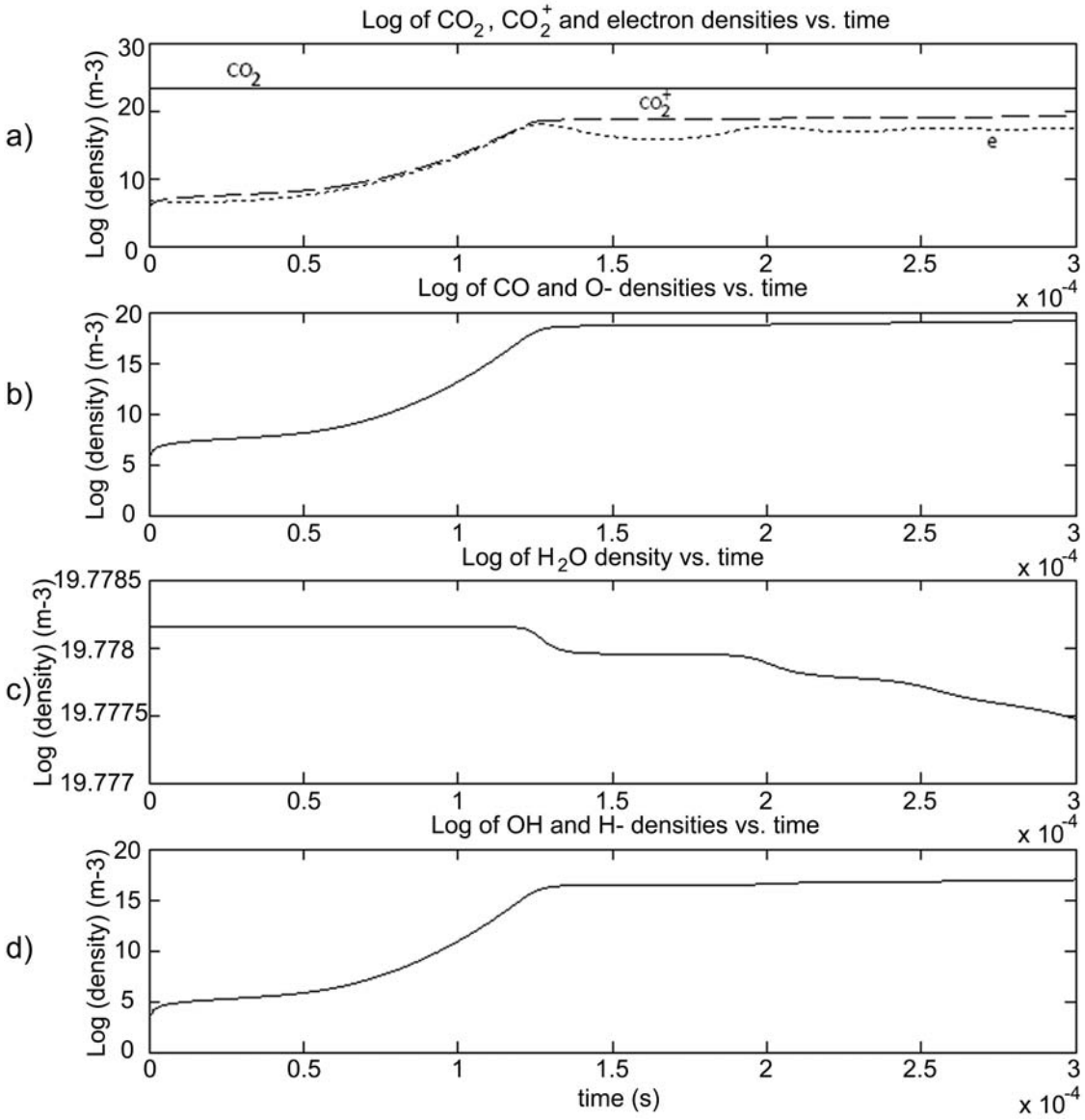

Figure 4. (a) Log of CO_2 density (solid), log of CO_2^+ density (dashed), and log of electron density (dotted) versus time. (b) Log of CO and O^- densities versus time. (c) Log of H_2O density versus time. (d) Log of OH and H^- densities versus time in seconds; all losses included.

Table 1. Electron Density, CO_2 Density, CO/O^- Densities, H_2O Density, OH and H^- Densities, CO_2^+ Density, and Density Change in CO_2 for Various Electric Field Ranges and a Dust Loss of $\eta = 0.031$ m^{-1} With Saturation via Intrinsic Chemistry[a]

E (kV/m)	n_e (m^{-3})	n_{CO_2} (m^{-3})	n_{CO}/n_{O^-} (m^{-3})	n_{H_2O} (m^{-3})	n_{OH}/n_{H^-} (m^{-3})	$n_{CO_2^+}$ (m^{-3})	Δn_{CO_2} (m^{-3})
5	4.54×10^{-14}	2×10^{23}	4.58×10^{6}	6×10^{19}	2.04×10^{3}	3.79	0
10	8.56×10^{-18}	2×10^{23}	4.92×10^{6}	6×10^{19}	1.34×10^{4}	1.27×10^{5}	0
12	7.73×10^{12}	2×10^{23}	4.28×10^{12}	6×10^{19}	2.58×10^{10}	1.24×10^{13}	-1.06×10^{14}
12.5	1.78×10^{16}	1.99×10^{23}	5.2×10^{18}	6×10^{19}	3.37×10^{16}	5.73×10^{18}	-1.12×10^{19}
13	1.52×10^{16}	1.99×10^{23}	5.21×10^{18}	5.99×10^{19}	3.15×10^{16}	5.39×10^{18}	-1.06×10^{19}
15	2.18×10^{17}	1.99×10^{23}	1.44×10^{19}	5.99×10^{19}	9.33×10^{16}	1.49×10^{19}	-2.9×10^{19}
20	4.33×10^{17}	1.99×10^{23}	5.65×10^{19}	5.95×10^{19}	4.44×10^{17}	5.94×10^{19}	-1.17×10^{20}
25	6.57×10^{17}	1.99×10^{23}	1.26×10^{20}	5.89×10^{19}	1.14×10^{18}	1.44×10^{20}	-2.7×10^{20}

[a]Density is in units of m^{-3}.

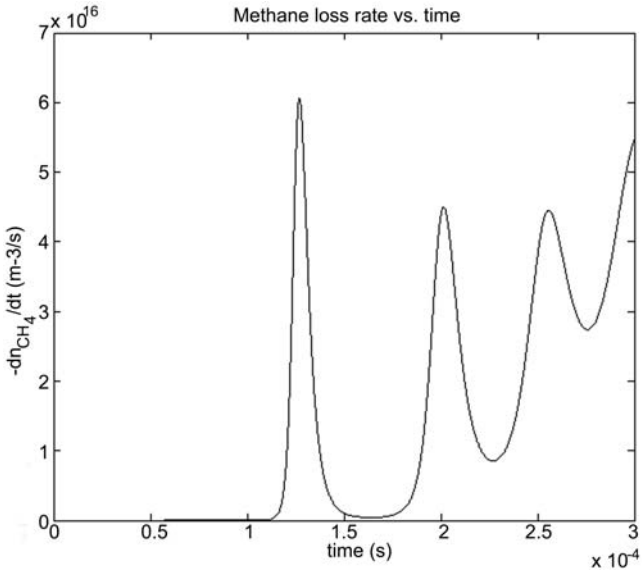

Figure 5. The methane density versus time in seconds for E = 15–20 kV/m and $\eta = 0.031$ m^{-1} with saturation via intrinsic chemistry.

to the DDEAM model, is calculated using the following equation, $\frac{\partial n_{CH_4}}{\partial t} = -k_{CH_4/e} n_{CH_4} n_e$, where n_e is the electron density calculated using DDEAM, n_{CH_4} is the methane density (assumed 10 ppb [*Mumma et al.*, 2004, 2009]), and $k_{CH_4/e}$ is the chemical rate at which methane is lost. The (e, CH_4) dissociative attachment cross section is large and extended in energy [*Ohmori et al.*, 1986], ranging from 10 to 100 eV. Peak values are at ~20 eV with a value of 1.6×10^{-20} m^2 and progressively decreased to about 1×10^{-20} m^2 at 100 eV. Using an approach similar to that of *Farrell et al.* [2006b], we find the chemical rate of methane dissociative attachment in E is then $k_{CH_4/e} = 1.9 \times 10^{-13}\, e^{-151708/E}$ m^3/s.

[31] Figure 5 shows the methane loss rate as a function of time derived from the DDEAM model, with all other parameters set for the nominal case with E = 15–20 kV/m and $\eta = 0.031$ m^{-1}. It can be seen in Figure 5 that methane is indeed lost in the electron gas. Comparing this density loss to that in Figure 2, we note that the loss of methane tracks the growth of electrons, with electron growth reaching a near-saturation level at 260 μs and methane loss becoming large also at that time. It is also noted that the loss rates ($\frac{dn_{CH_4}}{dt}$) from this model greatly exceed those of *Farrell et al.* [2006b] primarily because the saturated electron population at a given E field is larger than that applied in the other work.

[32] The entire preceding analysis assumed only a chemistry limit to electron growth, with saturation occurring when large portions of the available CO_2 chemical product needed to sustain electron growth (via impact ionization) begins to transform into the electron-recombining product CO_2^+. In other words, the fuel to drive the chemistry is transformed into a product that slows or stops the chemistry. The underlying assumption in the previous case is that the electron gas does not in any way shield the driving E field, which is valid for a low-density plasma. However, this assumption may not be valid when plasma densities become large. The next step below is addressing another possible limit to electron growth: saturation via space charge and the creation of a polarization electric field.

5. Saturation via Space Charge and Polarization Electric Field

[33] We now consider the effect the environmental currents have on the driving E field. Specifically, the change in E field from the plasma currents is derivable from the continuity equation as

$$\varepsilon_0 \frac{dE}{dt} = J_e - J_{CO_2^+} + J_{O^-} \tag{13}$$

where $J_e = n_e e v_d$, $J_{CO_2^+} = n_{CO_2^+} e v_{th}$ and $J_{O^-} = n_{O^-} e v_{th}$ where v_D is the electron drift velocity (2×10^5 m/s in large fields) and v_{th} is the thermal velocity of the molecules (~400 m/s). We assume that the net flux of ions in the column is defined by thermal flux loss into the ground. If however, the ground is not there (open-ended bottom), then the ion drift speed of ~10 m/s would be used. Both cases were tested and were found to yield nearly identical results on these time scales. Equation (13) was then placed in DDEAM and the E field starting at E_{min} was allowed to evolve in cadence with the forming plasma currents.

[34] A comparable experiment might be to take two parallel plates and place a voltage on them to create the necessary field. This will trigger the electron avalanche, but also creates the currents that naturally limit the E field. As a consequence, some level of quenching of the electron growth should occur.

[35] Unlike the intrinsic chemistry case, we will initially set the E field at a steady value, E_o, and then examine the effect of the reducing polarizing E field formed by the plasma. The resulting E field for the intermediate case (E_o = 20 kV/m) is shown in Figure 6 (along with the polarization

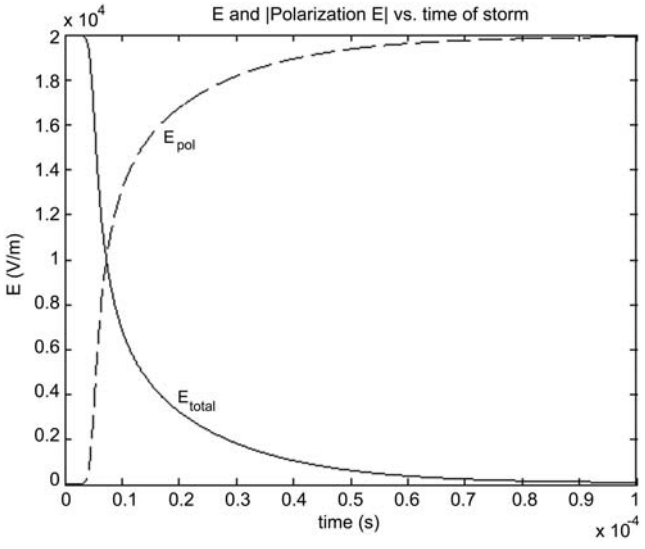

Figure 6. The evolution of the electric field with the inclusion of space charge currents (solid) and the polarization electric field (dashed) versus time.

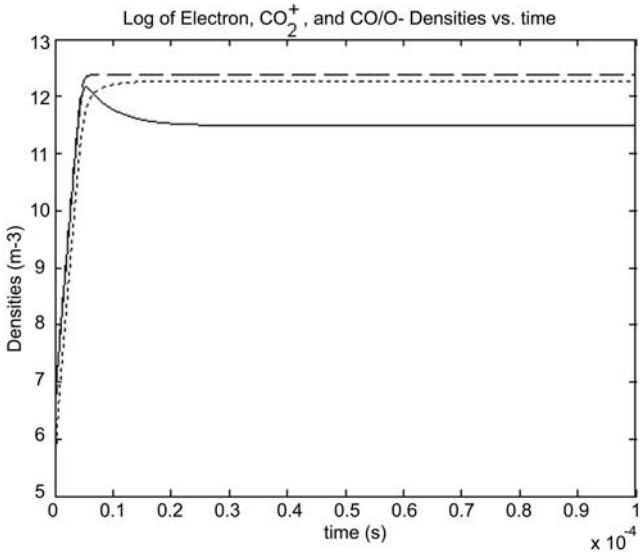

Figure 7. The evolution of electrons (solid), negative ions (dotted), and CO_2^+ (dashed) for polarization electric field/space charge.

E field) and the resulting derived chemistry is shown in Figure 7. As shown in Figure 7, a new equilibrium is created with steady state $n_e \sim 3 \times 10^{11}/m^3$, $n_{CO_2^+} = 2.4 \times 10^{12}/m^3$, and $n_{O^-} = 1.8 \times 10^{12}/m^3$. Note in Figure 6 that the *E* field undergoes a very quick decrease to low values, indicating that the space charge in the plasma is capable of self-shielding the driving *E* field. The electron drift velocity that varies directly with E ($v_d \sim 10 \cdot E$ in m/s) also decreases to small values with decreasing E keeping the plasma currents $n_e e v_d$ below 40 mA/m^2 and ~30 μA/m^2 at the end of the run.

[36] In this case, the system shuts itself off due to the effect of space charge in the constant *E* field, but this effect is most likely not realistic. We note that in a more realistic model, the final stabilized *E* field would not be zero but instead be defined by the balance between upward directed negatively tribocharged dust and the plasma. In the model herein we do not include the tribocharged dust in the generation of the initial *E* field (we assume the dust has already created the charge centers) and we then see how the gas reacts to the stress. Clearly, the next modification to the model will be the inclusion of the tribocharged dust currents in the system that then creates the *E* field. We can then arrive at the stabilized *E* field where there is a current balance between the tribocharged dust currents (moving downward) and electron currents (moving upward).

[37] Table 2 shows the final species values when limited by space charge effects. Examining the final ion and electron densities we conclude that there is a new chemistry "set point" for the space charge saturation process, with ionized gas densities about a factor of 10^8 lower than the saturation point obtained via chemical processes alone (Table 1). Clearly the effect of space charge is important to consider and strongly modifies the growth of the electron gas. In this new case, the electron growth is not limited by recombination, but instead is stunted by the effect of space charge and its action to offset the driving electric force [*Farrell et al.*, 2006a]. We also note that for this saturation case, plasma densities are more similar to levels described previously by *Delory et al.* [2006] and *Kok and Renno* [2008]. In the models, the electron growth path length is limited to 40–50 cm. However, in the model herein, the path length for growth is set to a very large value, but space charge sets the saturation values to levels more comparable to the path length limited cases.

[38] The methane loss rate, which was discussed earlier, is now calculated with the polarization electric field applied as the saturation mechanism. Figure 8 shows the methane loss rate as a function of time derived from the DDEAM model, with all other parameters set for the nominal case with E = 20 kV/m and $\eta = 0.031$ m^{-1}. As evident the methane loss rate is substantially slower than the preceding CO_2^+ recombination saturation case shown in Figure 5. In this new case, the loss is approximately $\frac{dn_{CH_4}}{dt}$ of $-10^{10}/m^3$ s and is comparable to the methane loss rates calculated previously by *Farrell et al.* [2006b]. Comparing this loss rate to the electron density in Figure 7, we note that the loss of methane tracks the growth of electrons as it did in the saturation via intrinsic chemistry case. As the polarization *E* field increases, and the overall ambient *E* field decreases in Figure 6, the number of electrons in the tail of the energy distribution $f(u, E)$ greatly reduces. With fewer electrons above 10 eV, the dissociative attachment of methane is reduced.

6. Conclusion

[39] We formulated and solved nine one-dimensional differential equations describing the new plasma chemistry in Martian dust storms and now refer to this system as the dust devil electron avalanche model (DDEAM). This sys-

Table 2. Electron Density, CO_2 Density, CO/O$^-$ Densities, H_2O Density, OH and H$^-$ Densities, CO_2^+ Density, and Density Change in CO_2 for Various Electric Fields and a Dust Loss of $\eta = 0.031$ m^{-1} With Saturation via Space Charge and Polarization *E* Field[a]

E (kV/m)	n_e (m^{-3})	n_{CO_2} (m^{-3})	n_{CO}/n_{O^-} (m^{-3})	n_{H_2O} (m^{-3})	n_{OH}/n_{H^-} (m^{-3})	$n_{CO_2^+}$ (m^{-3})	Δn_{CO_2} (m^{-3})
5	0.0113	2×10^{23}	4.87×10^6	6×10^{19}	1.83×10^3	0.24	0
10	9.9×10^{-24}	2×10^{23}	4.92×10^6	6×10^{19}	1.32×10^4	5.83×10^4	0
12	1.86×10^{-27}	2×10^{23}	5.38×10^6	6×10^{19}	2.0×10^4	5.36×10^5	0
12.5	7.59×10^{-27}	2×10^{23}	5.71×10^6	6×10^{19}	2.27×10^4	8.76×10^5	0
13	3.64×10^{-25}	2×10^{23}	6.26×10^6	6×10^{19}	2.64×10^4	1.43×10^6	0
15	1.79	2×10^{23}	3.47×10^7	6×10^{19}	1.78×10^5	3.02×10^7	0
20	3.08×10^{11}	2×10^{23}	1.88×10^{12}	6×10^{19}	7.14×10^9	2.37×10^{12}	-4.25×10^{12}
25	8.04×10^{12}	2×10^{23}	2.45×10^{12}	6×10^{19}	1.19×10^{10}	1.43×10^{13}	-1.68×10^{13}

[a]Density is in units of m^{-3}.

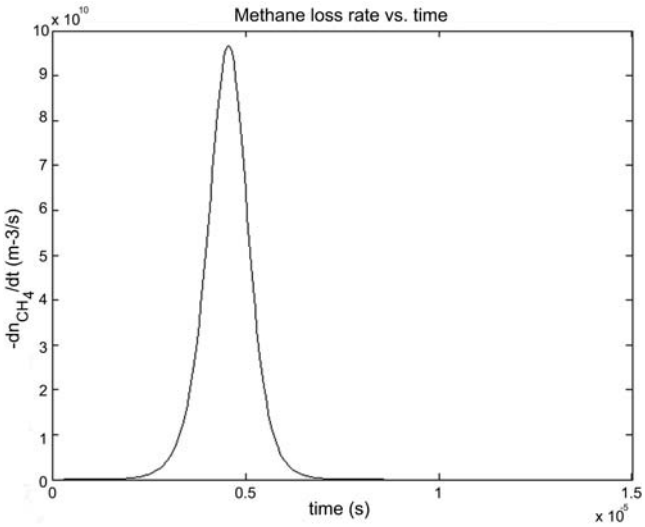

Figure 8. The methane density versus time in seconds for E = 20 kV/m and $\eta = 0.031$ m^{-1} with saturation via space charge and polarization E field. Note that the time scale has been shortened to 15 μs.

tem solves the continuity equations that characterize the electron density, as well as the densities of the constituents and their products due to electron/molecule interactions in the Martian atmosphere. This includes the evolution of the densities of CO_2, CO_2^+, CO, O^-, H_2O, OH, H^- and CH_4 under a driving electric field. We can also modify this driving field under the influence of space charge.

[40] Given a driving electric field, the DDEAM model follows the evolution of electrons and atmospheric molecules including impact ionization (source), dissociative attachment (loss), recombination (loss), and dust absorption (loss). The results of the modeling include the following.

[41] 1. For E fields above about 12 kV/m, the electron avalanche process is initiated (electron impact ionization exceeds attachment and dust losses) and continues for 30–100 μs.

[42] 2. However, the avalanche process does not continue indefinitely, and is saturated (becomes stabilized to equilibrium) either through electron recombination with CO_2^+ ions or with a polarization E field created by the plasma space charge.

[43] 3. When the electron density stabilizes, the dominant negative charge carrier is (surprisingly) not the electrons but O^- formed from electron dissociative attachment with CO_2 (into CO and O^-). The ionized gas thus consists of CO_2^+ and O^- of comparable levels and electrons form a secondary population with a concentration ~10% of the O^-.

[44] 4. The concentrations of chemical products are different depending upon the assumed saturation process. Intrinsic chemical saturation produced an ionized gas density in equilibrium at 10^{-3} that of the neutral gas while the ionized component produced under the influence of space charge is limited to 10^{-10} that of the neutral gas.

[45] The saturation via space charge tends to turn the entire process off, leaving only a short-lived transient. In fact, if we placed parallel plates in the low-pressure CO_2 gas, we might consider this transient as a sort of short-circuit discharge formed between the plates. It is not a full breakdown, but instead a glow-like discharge that might resemble the step leader of a lighting discharge. However, if we included a triboelectric current source, there would be a maintenance of the E field generator and the overall steady state E field would reflect the equilibrium between the dust currents and opposing space charge currents that form in larger E fields.

[46] We consider both chemistry and electrical saturation scenarios since we do not ultimately know the dominant, defining saturation mechanism. We leave open the distinct possible existence of saturation processes not considered herein, making this work intrinsically nonunique, but still a next obvious step from the pathfinding Delory/Atreya work.

[47] The formation of a large concentration of energetic negative O ions near the surface is itself interesting. Through grain surface triboelectric effects, the surface interface should be charged positive creating a natural attraction between the O^- ions concentrated at the bottom of the dust devil/storm. The surface, which has undergone abrasion by the saltating dust should also have unsatisfied chemical bonds that combine with the O^- ions. Hence, we leave open the distinct possibility of new O^- chemistry occurring at the surface, forming more complicated oxides at exposed interfaces. Any surface chemistry is beyond the scope of this current work, but represents a suggestive avenue of future research.

Appendix A: Calculating the Chemical Rate

[48] Given the electron energy distribution function $f(u, E) = f_o(u_o)e^{-2.3B(u-u_o)/E}$, the reaction rate k can be calculated using the following expression:

$$k = \langle \sigma v \rangle = \left(\frac{2e}{m_e}\right)^{1/2} \int \sigma(u) u f(u) du \tag{A1}$$

where σ is the collision cross section for a given process (i.e., electron impact ionization, electron dissociative attachment etc.) and $v = \left(\frac{2e}{m_e}\right)^{1/2} u^{1/2}$.

[49] The chemical rate for ionization of carbon dioxide is give by the following equation [*Rees*, 1981]:

$$k_i = \left(\frac{2e}{m_e}\right)^{1/2} \int_{u_i}^{\infty} \sigma_i(u) u f(u, E) \partial u \tag{A2}$$

where σ_i is the ionization cross section (55), which is in the form of [*Jackson*, 2008]

$$\sigma_i = Au + C \tag{A3}$$

where A = 0.09 × 10^{-20} m^2/eV and C = −1.3 × 10^{-20} m^2 [*Jackson et al.*, 2008]. After solving the integral in (A2) and using the simple expressions for the electron energy distribution and the ionization cross section (A3), the chemical rate for ionization becomes

$$k_i = \left(\frac{2e}{m}\right)^{1/2} f_o e^{2.3\frac{B}{E}u_o} \frac{e^{-2.3\frac{B}{E}u_i}}{5.29B^2} E^2 A \left[\frac{2E}{2.3B} + u_i\right] \tag{A4}$$

[50] Note that k_i is a function of electric field. All other parameters are known values, with u_i being the ionization energy of 14.5 eV. Equation (A4) is then use to derive Townsend's first coefficient for electron impact ionization, $\alpha = n_N k_i/v_d$. The final derived expression is dependent on only a few variables that are known $\alpha = -{n_{CO_2}}^2 \sigma_{el} \frac{C}{B} e^{-2.3\frac{B}{E}u_i}$.

[51] The chemical rate for dissociative attachment of electrons to carbon dioxide is

$$k_{CO_2/e} \sim \left(\frac{2e}{m_e}\right)^{1/2} \sigma_d(u_d) u_d f_o e^{-2.3\frac{B(u_d-u_o)}{E}} \Delta u \qquad \text{(A5)}$$

where $\sigma_d = 0.15 \times 10^{-22}$ m^2, $\Delta u \sim 1$ eV and $u_d \sim 4.4$ eV [*Itikawa*, 2002; *Delory et al.*, 2006]. The chemical rate equation can then be expressed as [*Jackson*, 2008]

$$k_{CO_2/e} = 0.39 \times 10^{-16} e^{-12493/E} \text{ m}^3/\text{s} \qquad \text{(A6)}$$

[52] Note that $k_{CO_2/e}$ is also a function of electric field and all other parameters are known values. In the same manner, the chemical rate for electron dissociative attachment of H_2O is found. The dissociation energy for H_2O is ~6.5 eV. The cross section at this energy is given as $\sigma_{H_2O}(u_d) = 0.64 \times 10^{-21}$ m^2 [*Itikawa*, 2002; *Delory et al.*, 2006]. The chemical rate equation for H_2O can then be expressed as [*Jackson*, 2008]

$$k_{H_2O/e} = 0.25 \times 10^{-14} e^{-321264/E} \text{ m}^3/\text{s} \qquad \text{(A7)}$$

[53] The chemical rate for electron/CO_2^+ recombination is described as

$$k_r = A\left(\frac{T}{300}\right)^{\alpha} e^{-\beta/T} \text{ cm}^3/\text{s} \qquad \text{(A8)}$$

where T is the temperature of the electron distribution in kelvins, A is a transition probability constant between (3–6) $\times 10^7$/s, and α and β are constants specific to the ion and have values of −0.5 and 0, respectively, for CO_2 [*Prasad and Huntress*, 1980]. We assume an electron temperature near 1200 K based on the form of the distribution functions. While there is a functional dependence of Te with E field, k_r varies as $T^{-1/2}$ making the dependency very mild (quasi-constant) in expression (A8).

[54] The drift velocity (v_D), is found using the expression $v_D = [{}^{-2}/_3 \frac{e}{m_e} \int_0^{\infty} \frac{u^{3/2}}{\nu_c} \frac{\partial f(u,E)}{\partial u} du]E$, and simplifies to [*Jackson*, 2008]

$$v_D = \left(\frac{2e}{m_e}\right)^{1/2} f_o \frac{e^{2.3Bu_o/E}}{3\sigma_{el} n_{CO_2}} \frac{E^2}{2.3B} \qquad \text{(A9)}$$

where ν_c is the mean collision frequency, $e = 1.6 \times 10^{-19}$ C, $m_e = 9 \times 10^{-31}$ kg, $\sigma_{el} = 0.84 \times 10^{-19}$ m^2 [*Itikawa*, 2002]. The drift velocity, for E fields above 5 kV/m, approaches a constant of $v_d \sim 2 \times 10^5$ m/s because the exponential term almost completely offsets the increasing E^2 for large E.

[55] **Acknowledgments.** We gratefully acknowledge support from the Mars Fundamental Research Program and the NASA co-op program at the Goddard Space Flight Center.

References

Atreya, S. K., et al. (2006), Oxidant enhancement in Martian dust devils and storms: Implications for life and habitability, *Astrobiology*, *6*(3), 439–450, doi:10.1089/ast.2006.6.439.

Chen, F. F. (1984), *Introduction to Plasma Physics and Controlled Fusion*, vol. 1, *Plasma Physics*, 2nd ed., Plenum, New York.

Crozier, W. D. (1964), The electric field of a New Mexico dust devil, *J. Geophys. Res.*, *69*(24), 5427–5429, doi:10.1029/JZ069i024p05427.

Delory, G. T., et al. (2006), Oxidant enhancement in Martian dust devils and storms: Storm electric fields and electron dissociative attachment, *Astrobiology*, *6*(3), 451–462, doi:10.1089/ast.2006.6.451.

Desch, S. J., and J. N. Cuzzi (2000), The generation of lightning in the solar nebula, *Icarus*, *143*, 87–105, doi:10.1006/icar.1999.6245.

Eden, H. F., and B. Vonnegut (1973), Electrical breakdown caused by dust motion in low-pressure atmospheres: Consideration for Mars, *Science*, *180*(4089), 962–963, doi:10.1126/science.180.4089.962.

Ette, A. I. I. (1971), The effect of the Harmattan dust on atmospheric electric parameters, *J. Atmos. Terr. Phys.*, *33*, 295–300, doi:10.1016/0021-9169(71)90208-X.

Farrell, W. M., M. L. Kaiser, M. D. Desch, J. G. Houser, S. A. Cummer, D. M. Wilt, and G. A. Landis (1999), Detecting electrical activity from Martian dust storms, *J. Geophys. Res.*, *104*(E2), 3795–3801, doi:10.1029/98JE02821.

Farrell, W. M., G. T. Delory, S. A. Cummer, and J. R. Marshall (2003), A simple electrodynamic model of a dust devil, *Geophys. Res. Lett.*, *30*(20), 2050, doi:10.1029/2003GL017606.

Farrell, W. M., et al. (2004), Electric and magnetic signatures of dust devils from the 2000–2001 MATADOR desert tests, *J. Geophys. Res.*, *109*, E03004, doi:10.1029/2003JE002088.

Farrell, W. M., N. Renno, G. T. Delory, S. A. Cummer, and J. R. Marshall (2006a), Integration of electrostatic and fluid dynamics within a dust devil, *J. Geophys. Res.*, *111*, E01006, doi:10.1029/2005JE002527.

Farrell, W. M., G. T. Delory, and S. K. Atreya (2006b), Martian dust storms as a possible sink of atmospheric methane, *Geophys. Res. Lett.*, *33*, L21203, doi:10.1029/2006GL027210.

Forward, K. M., D. J. Lacks, and R. M. Sankaran (2009), Particle-size dependent bipolar charging of Martian regolith simulant, *Geophys. Res. Lett.*, *36*, L13201, doi:10.1029/2009GL038589.

Freier, G. D. (1960), The electric field of a large dust devil, *J. Geophys. Res.*, *65*(10), 3504, doi:10.1029/JZ065i010p03504.

Itikawa, Y. (2002), Cross sections for electron collisions with carbon dioxide, *J. Phys. Chem. Ref. Data*, *31*(3), 749–767, doi:10.1063/1.1481879.

Jackson, T. L. (2008), Collisional plasmas in Martian dust storms: Application to sustenance and glow emissions, D.Eng. dissertation, Morgan State Univ., Baltimore, Md.

Jackson, T. L., and W. M. Farrell (2006), Electrostatic fields in dust devils: An analog to Mars, *IEEE Trans. Geosci. Remote Sens.*, *44*(10), 2942–2949, doi:10.1109/TGRS.2006.875785.

Jackson, T. L., W. M. Farrell, G. T. Delory, and J. Nithianandam (2008), Effect of dust absorption on the electron avalanche process occurring within Martian dust storms, *Geophys. Res. Lett.*, *35*, L16201, doi:10.1029/2008GL034523.

Klimas, A. J., and W. M. Farrell (1994), A splitting algorithm for Vlasov simulation with filamentation filtration, *J. Comput. Phys.*, *110*(1), 150–163, doi:10.1006/jcph.1994.1011.

Kok, J. F., and N. O. Renno (2008), Electrostatics in wind-blown sand, *Phys. Rev. Lett.*, *100*, 014501, doi:10.1103/PhysRevLett.100.014501.

Kok, J. F., and N. O. Renno (2009), Electrification of wind-blown sand on Mars and its implications for atmospheric chemistry, *Geophys. Res. Lett.*, *36*, L05202, doi:10.1029/2008GL036691.

Melnik, O., and M. Parrot (1998), Electrostatic discharge in Martian dust storms, *J. Geophys. Res.*, *103*(A12), 29,107–29,117, doi:10.1029/98JA01954.

Mills, A. A. (1977), Dust clouds and frictional generation of glow discharges on Mars, *Nature*, *268*, 614, doi:10.1038/268614a0.

Mumma, M. J., R. E. Novak, M. A. DiSanti, B. P. Bonev, and N. Dello Russo (2004), Detection and mapping of methane and water on Mars, *Bull. Am. Astron. Soc.*, *36*(4), Abstract 26.02.

Mumma, M. J., et al. (2009), Strong release of methane on Mars in northern summer 2003, *Science*, *323*(5917), 1041–1045, doi:10.1126/science.1165243.

Nighan, W. L. (1970), Electron energy distributions and collision rates in electrically excited N_2, CO, and CO_2, Phys. *Rev. A Gen. Phys.*, *2*(5), 1989–2000, doi:10.1103/PhysRevA.2.1989.

Ohmori, Y., K. Kitamori, M. Shimozuma, and H. Tagashira (1986), Boltzmann equation analysis of electron swarm behaviour in methane, *J. Phys. D Appl. Phys.*, *19*, 437–455, doi:10.1088/0022-3727/19/3/013.

Pitchford, L. C., S. V. O'Neil, and J. R. Rumble Jr. (1981), Extended Boltzmann analysis of electron swarm experiments, *Phys. Rev. A Gen. Phys.*, *23*(1), 294–304, doi:10.1103/PhysRevA.23.294.

Prasad, S. S., and W. T. Huntress Jr. (1980), A model for gas phase chemistry in interstellar clouds: I. The basic model, library of chemical reactions, and chemistry among C, N, and O compounds, *Astrophys. J. Suppl. Ser.*, *43*, 1–35, doi:10.1086/190665.

Rees, J. A. (1981), Basic processes of electrical discharges, in *Electrical Breakdown and Discharges in Gases. Part A: Fundamental Processes and Breakdown*, edited by E. E. Kunhardt and L. H. Luessen, pp. 73–107, Plenum, New York.

Zhai, Y., S. A. Cummer, and W. M. Farrell (2006), Quasi-electrostatic field analysis and simulation of Martian and terrestrial dust devils, *J. Geophys. Res.*, *111*, E06016, doi:10.1029/2005JE002618.

G. T. Delory, Space Sciences Laboratory, University of California, Berkeley, CA 94720, USA.

W. M. Farrell and T. L. Jackson, Solar System Exploration Division, NASA Goddard Space Flight Center, Greenbelt, MD 20771, USA. (telana.l.jackson@nasa.gov)

J. Nithianandam, Department of Electrical Engineering, Morgan State University, Baltimore, MD 21251, USA.